The Aeronautical Journal (2025), 1–12
doi:10.1017/aer.2025.10071

ROYAL AERONAUTICAL SOCIETY

RESEARCH ARTICLE

Effect of bio-inspired leading-edge modifications on aerodynamic performance of a non-slender delta wing

D. Dikbaş[1], E. Güneş[1], G. Koçak[2] and M. M. Yavuz[1]

[1]Mechanical Engineering Department, Middle East Technical University, Ankara, Türkiye
[2]Turkish Aerospace Industries, Inc., Ankara, Türkiye
Corresponding author: M. M. Yavuz; Email: ymetin@metu.edu.tr

Received: 23 March 2025; **Revised:** 13 August 2025; **Accepted:** 13 August 2025

Keywords: bio-inspired wing modifications; experimental aerodynamics; non-slender delta wing; passive flow control

Abstract

The effect of the bio-inspired leading-edge modifications on the aerodynamic performance of non-slender delta wing models was investigated in a low-speed wind tunnel using force and surface pressure measurements. The measurements were performed at a Reynolds number of $Re = 1 \times 10^5$ over an angle-of-attack range from -4° to 30°. Seven different sharp-edged delta wing models with a 45-degree sweep angle (Λ), including a base wing, were used to study the effect of sinusoidal and saw-tooth leading-edge modifications. Sinusoidal leading-edge wing designs were inspired by the leading-edge tubercles of the humpback whale's pectoral fins. The results indicate that the bio-inspired wing modifications resulted in a delay in the stall angle by 4 degrees, smoother stall characteristics, a higher maximum lift coefficient, and increased post-stall lift. The drag coefficient of the modified wings was observed as higher than that of the base wing model. Regarding the longitudinal static stability, leading-edge modifications decreased the stability of the wing as the angle-of-attack surpassed $\alpha = 17^\circ$.

Nomenclature

MAV	micro air vehicles
NACA	National Advisory Committee for Aeronautics
NASA	National Aeronautics and Space Administration
PIV	particle image velocimetry
SLE	sinusoidal leading-edge
UCAV	unmanned combat air vehicles
UAV	unmanned aerial vehicle
A	reference area
C	chord
C_D	drag coefficient
C_L/C_D	lift-to-drag ratio
C_L	lift coefficient
$C_{L\,\max}$	maximum lift coefficient
C_M	pitching moment coefficient
$C_{M\,at\,TE}$	moment coefficient at the trailing edge
C_p	surface pressure coefficient
F_D	drag force
F_L	lift force
L	reference length
P_{dyn}	dynamic pressure of the freestream
P_m	mean pressure
P_∞	static pressure of the freestream

https://doi.org/10.1017/aer.2025.10071 Published online by Cambridge University Press

Re	Reynolds number
S	span
t	thickness
U_∞	free stream velocity
x/C	chordwise distance

Greek symbol

α	angle-of-attack
Λ	sweep angle
ρ	density
ϕ/C	amplitude ratio
λ/C	wavelength ratio

1.0 Introduction

Delta wings are commonly used on unmanned aerial vehicles (UAV), micro air vehicles (MAV), and unmanned combat air vehicles (UCAV) due to their ability to maintain attached flow on the wing surface at high angles of attack, which, as a result, enhances the lift coefficient and delays stall [9, 26]. In recent years, there has been an increased demand for these aerial vehicles in the civilian and military sectors. This heightened interest increased the popularity of research on the flow control of delta wings.

Delta wings are classified into two categories according to their sweep angles (Λ): slender ($\Lambda > 55°$) and non-slender ($\Lambda < 55°$) delta wings [11]. In non-slender delta wings, a dual primary vortex structure is generated due to the proximity of the vortex formation to the wing surface [10, 12]. Extensive studies have been conducted to improve the aerodynamic performance of these wings with passive and active flow control methods. Bio-inspired structures such as leading-edge serrations, riblets, surface topography, grooves, vortex generators, such as needle-shaped vortex generators, and leading-edge tubercles are studied by many researchers as passive flow control methods [23, 28, 29].

Otto Lilienthal [17] conducted one of aviation's earliest and most influential studies on biomimicry. In his research, he mimicked various wing shapes and movements of different bird species to make human flight possible. Many researchers [16, 23, 27, 29] and engineers followed the same path and researched avians to design or improve aerial vehicles. However, avians are just one source of inspiration for aerodynamics research. Structures from aquatic animals, insects and even plants can be utilised to improve aerodynamic performance [28].

Recently, marine animals have received attention from researchers. These researchers have investigated the effects of various marine animal structures, such as fish scales, skin topography, and leading-edge tubercles, to decrease drag, delay transition, and improve aerodynamic efficiency [1, 5, 22].

Among these structures, the tubercles of humpback whales have particular importance, since these structures serve as vortex generators and improve the whale's manoeuverability in the water [6, 20, 25, 31]. Most of the studies investigating the effects of these structures study the effect of the sinusoidal leading edge (SLE) on aerofoils, while a few investigate the effects of SLE on delta wings. These studies mainly focused on the effect of amplitude and wavelength on the aerodynamic or hydrodynamic performance of SLE models. Other researchers studied the effect of sinusoidal leading-edge modifications with visualisation methods such as particle image velocimetry (PIV) [4, 7], tuft flow visualisation [14], hydrogen-bubble visualisation [3], and surface oil-flow visualisation [3, 25, 33].

Johari et al. [14] were among the first research groups to focus on aerofoils with sinusoidal leading-edge modifications inspired by humpback whale tubercles. They conducted force measurements and the tuft flow visualisation method to investigate the effects of SLE modifications on the aerodynamic performance and flow characteristics of a NACA 63_4-021 aerofoil. The results of this study showed that the aerofoils with SLE modifications did not exhibit similar stall characteristics compared to the baseline aerofoil. Moreover, the results showed that the poststall lift coefficients were approximately

https://doi.org/10.1017/aer.2025.10071 Published online by Cambridge University Press

1.5 times higher when SLE modifications were utilised. Guerreiro and Sousa [8] investigated the aerodynamic performance of the NASA LS(I)-0417 profile with SLE modifications at Reynolds numbers of $Re = 0.7 \times 10^5$ and $Re = 1.4 \times 10^5$. The results of this study indicated that the wings with SLE modifications are less prone to performance deterioration due to variation in Reynolds number than wings with no modifications [8]. Hansen et al. [13] studied the effect of SLE on a NACA 0021 aerofoil without any sweep or taper and compared two-dimensional and three-dimensional models of this aerofoil at $Re = 1.2 \times 10^5$. This study indicated that the presence of tubercles had insignificant effects on the formation of the wing-tip vortices. The smallest amplitude and smallest wavelength configuration of tubercles performed the best for both two-dimensional and three-dimensional cases [13]. Van Nierop et al. [30] experimentally studied the SLE modifications on a swept wing. The maximum lift coefficient of the SLE wing models was observed to be higher than that of the base wing in the post-stall regime. Furthermore, for wing models with lower amplitude perturbations, the transition to stall occurs more gradually compared to the base wing model.

Yoon et al. [31] numerically studied the hydrodynamic characteristics of SLE modifications on the NACA 0020 aerofoil with various waviness ratios at $Re = 2 \times 10^6$. The results of this study showed that as the waviness increases, the stall occurs earlier than that of the base model. However, the wings with SLE modifications had a higher lift coefficient in the post-stall region. Furthermore, it was observed that irrespective of the waviness ratio, the effect of SLE modifications on the flow structure was insignificant for the lower angles of attack ($0^\circ \leq \alpha \leq 12^\circ$) [31]. Kim et al. [15] conducted similar research with Yoon et al. and reached the same verdict. Zhao et al. [32] conducted a large eddy simulation (LES) on a NACA 0021 aerofoil with and without SLE modifications and studied the effect of amplitude on the flow structure at $Re = 1.2 \times 10^6$. The results of his study indicated that the flow separation was delayed and the aerodynamic performance was improved for large amplitudes due to the separation bubbles caused by the turbulent mixing. Moscato et al. [21] conducted a numerical study to investigate the effects of SLE modifications on force coefficients, flow fields, turbulence production and flow reattachment. This study showed that using SLE modifications increased the maximum lift coefficient by approximately 20%, delayed the stall angle up to 4°, provided smoother post and pre-stall behaviour, reduced the level of turbulence production and prevented separation and backflow on the wing's upper surface. Moreover, the post-stall behaviour was smoother than the unmodified wing [21]. Ramakrishna et al. [26] compared the effects of leading-edge design on a delta wing with a sweep angle of $\Lambda = 65^\circ$. Three different leading-edge designs were used: plane delta wing, with no modifications, saw-tooth delta wing, and sinusoidal delta wing. The results showed that the saw-tooth wing model delayed stall more than the SLE wing models [26]. Lift coefficients for all the wing models were not significantly affected by variations in the Reynolds number. Moreover, the lift-to-drag ratio of the saw-tooth model was higher than other models. The sinusoidal wing model performed better than the plane wing regarding the lift-to-drag ratio, but did not exceed the saw-tooth wing model [26].

Chen et al. [3, 4] investigated the effects of SLE modifications on a delta wing with a sweep angle of $\Lambda = 52^\circ$. Nine different wing configurations were used to investigate multiple amplitudes and wavelengths. The force measurements showed results similar to those of Johari et al. [14]. The results indicated that when the amplitude was increased above a critical value, the maximum lift coefficient decreased significantly, and the stall was delayed when SLE modifications were utilised [3, 4]. Goruney and Rockwell [7] investigated the near-surface flow patterns of an SLE delta wing with a sweep angle of $\Lambda = 50^\circ$ at a Reynolds number of $Re = 1.5 \times 10^4$. The findings of this study showed that the focus of three-dimensional separation moved toward the leading edge as the amplitude of the SLE was increased. When the amplitude surpasses a critical point, the focus of three-dimensional separation is eliminated and replaced by a focus of attachment [7].

In the current study, the effect of bio-inspired leading-edge modifications on the flow structure over a non-slender delta wing with a sweep angle of $\Lambda = 45^\circ$ is studied experimentally at a Reynolds number of $Re = 1 \times 10^5$. Techniques such as force and surface pressure measurements were utilised over an angle-of-attack range from -4° to 30° and -2° to 30°, respectively. Four sinusoidal and two saw-tooth leading-edge wing models with wavelength ratios from 0.1 to 0.3 and amplitude ratios from 0.02 to 0.05 were compared with a base wing model.

https://doi.org/10.1017/aer.2025.10071 Published online by Cambridge University Press

2.0 Experimental methods

Experiments were conducted in a low-speed, suction-type, open-circuit wind tunnel in the Fluid Mechanics Laboratory of the Mechanical Engineering Department at Middle East Technical University. The wind tunnel has five main parts: a settling chamber, a contraction cone, a test section, a diffuser and a fan. The wind tunnel has two symmetrical inlet sections at the sides, with fine mesh screens. The contraction cone has a 2000 mm length and a contraction ratio of 8:1. The test section, which has transparent walls, has a 750 mm width, 510 mm height and 2000 mm length. An axial fan with a 10kW AC motor is assembled at the exit of the wind tunnel with a remote control unit to control the velocity of the test section. The test section has a maximum freestream velocity of 20 m/s. The force and surface pressure measurements were performed at a Reynolds number of $Re = 1 \times 10^5$ with a corresponding free stream velocity range of $10.9 \leq U_\infty \leq 11.2$. The maximum blockage ratio is lower than 3% at the highest angle-of-attack of $\alpha = 30°$.

Seven different sharp-edged delta wing models were used with a 45-degree sweep angle (Λ) and a single-sided bevel on the windward side at a 45-degree angle. Sinusoidal and saw-tooth leading-edge modifications were applied in the present study. The schematics and pictures of some of the wing models are shown in Fig. 1. The sinusoidal-leading-edge wing models were inspired by the tubercle structure of humpback whales, and saw-tooth leading-edge models were inspired by the studies of Ramakrishna et al. [26]. The wavelength and amplitude ratios of the wing models are given in Table 1. The 'S' and 'ST' notations in the names of the wing models represent sinusoidal and saw-tooth leading edges, respectively. The 'λ' symbol denotes the wavelength ratio, while the 'ϕ' symbol represents the amplitude ratio, and the numbers following these symbols indicate decimal values of ratios. The chord (C), the span (S) and the thickness (t) of the delta wing models are 135, 270, and 8 mm, respectively. The surface area of each modified wing model is kept the same as that of the base wing. The delta wing models were designed to allow access to the pressure channels from the trailing edge. There are nine pressure channels in each half of the wing, eighteen pressure channels in total, at a chordwise distance of $x/\mathrm{C} = 0.5$ for each wing model.

The aerodynamic force measurements were performed using an ATI Gamma Series Force/Torque transducer calibrated according to the SI-32-2.5 scheme. The wing model is assembled to a strut that connects at its trailing edge, aligning it with the transducer's y-axis, which acts as the pitch axis. The strut is connected to the sensor adaptor, and the sensor is rigidly connected to the model positioning system. The model positioning system is a traverse system that allows users to change the angle-of-attack of the wind model with a desired increment. The force measurements were performed over an angle-of-attack range of $-4°$ to $30°$. The drag and lift coefficients (C_D, C_L) and the pitch moment coefficient (C_M) were calculated using Equations (1) and (2), where the reference area (A) is 18,225 mm^2, and the reference length (L) is equal to the wing chord length (C), which is 135 mm. Measurements were sampled with a National Instruments NI-PCIe-6321 16-bit data acquisition (DAQ) card at 10 kHz for 10 seconds for each measurement. Maximum absolute uncertainty values for lift coefficient (C_L), drag coefficient (C_D), moment coefficient (C_M) and lift-to-drag ratio (C_D/C_L) are estimated as ± 0.05, ± 0.05, and ± 0.06, respectively. A schematic view of the wind tunnel from the top and end view, with the force measurement setup, is given in Fig. 2.

$$C_D, C_L = \frac{F_D, F_L}{\frac{\rho U_\infty^2}{2} A} \tag{1}$$

$$C_M = \frac{M_y}{\frac{\rho U_\infty^2}{2} AL} \tag{2}$$

The aerodynamic and gravitational forces and moments of the bare strut are measured for each angle-of-attack to tare out the effects of the strut system.

https://doi.org/10.1017/aer.2025.10071 Published online by Cambridge University Press

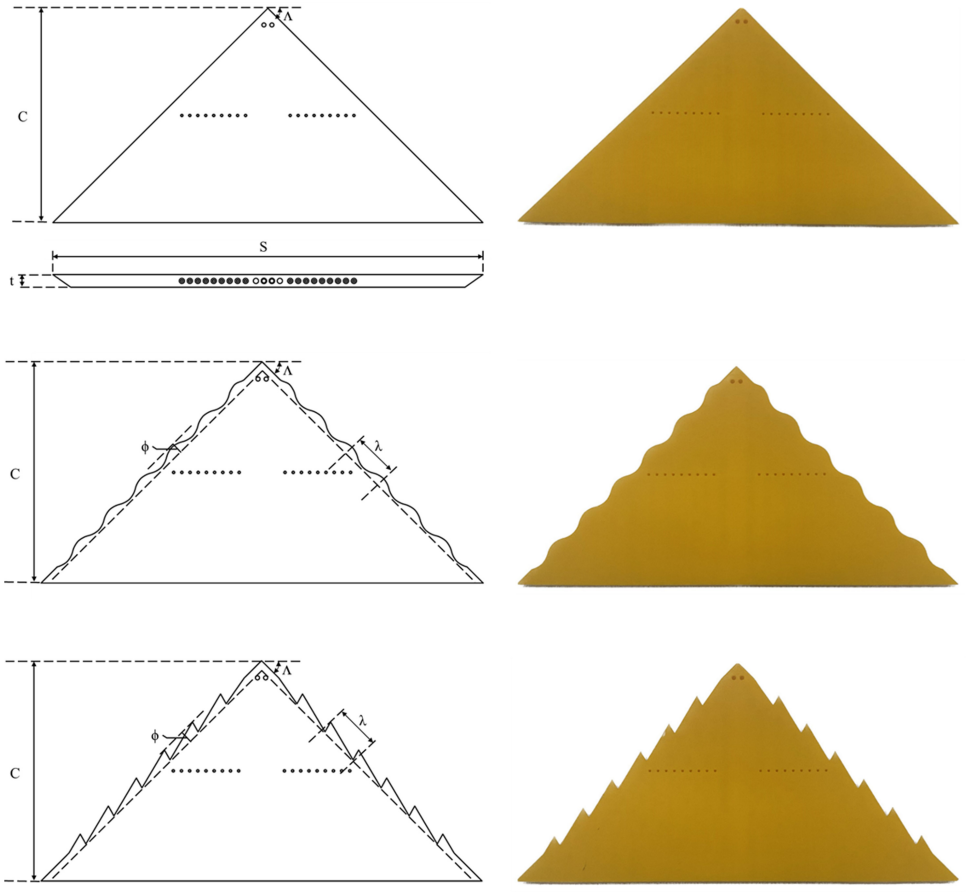

Figure 1. *Schematics and pictures of the base, sinusoidal leading-edge and saw-tooth leading-edge wing models.*

Table 1. *Wavelength and amplitude ratios for sinusoidal and saw-tooth leading edge wings*

Model	λ/C	ϕ/C
S-λ1ϕ02	0.1	0.02
S-λ2ϕ03	0.2	0.03
S-λ2ϕ05	0.2	0.05
S-λ3ϕ05	0.3	0.05
ST-λ2ϕ03	0.2	0.03
ST-λ2ϕ05	0.2	0.05

The surface pressure measurements were conducted on the suction side of all the wing models with a 16-channel Netscanner 9116 Intelligent Pressure Scanner. This scanner is capable of measuring pressures in the range of 0–2.5 kPa with 16 piezo-resistive transducers. The resolution of the pressure scanner is ±0.003% FS (full scale), and the scanner's accuracy is ±0.05% FS. The resolution of the pressure scanner is ensured with the microprocessor and temperature sensors, which are integrated into the pressure scanner to compensate for the thermal effects, nonlinearity, sensitivity and transducer outputs for offset.

https://doi.org/10.1017/aer.2025.10071 Published online by Cambridge University Press

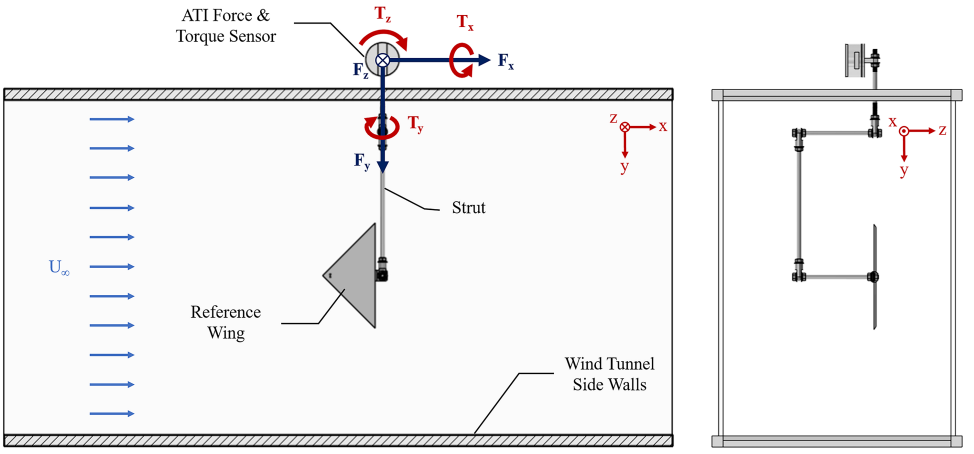

Figure 2. *Schematic representation of the top and end views of the force measurement system.*

The pressure data were collected over an angle-of-attack range of -2° to 30° and for 10 seconds at a sampling rate of 500 Hz. The pressure coefficient C_p was calculated using Equation (3). The maximum absolute uncertainty value for the pressure coefficient (C_p) is estimated as 2.5%.

$$C_p = \frac{P_m - P_\infty}{\frac{\rho U_\infty^2}{2}} = \frac{P_m - P_\infty}{P_{dyn}} \tag{3}$$

3.0 Results and discussion

In this study, force and surface pressure measurements were performed on seven wing models. Four of these wing models, the base wing, S-λ2ϕ03, S-λ2ϕ05 and ST-λ2ϕ05, were selected and presented based on their performance.

3.1 Results of force measurements

The results of the force measurements are presented as distributions of aerodynamic coefficients with respect to the angle-of-attack. In Fig. 3, the drag coefficient (C_D), lift coefficient (C_L), moment coefficient at the trailing edge ($C_{M\,at\,TE}$), and the lift-to-drag ratio (C_L/C_D) at various angles of attack for the base wing, S-λ2ϕ03, S-λ2ϕ05 and ST-λ2ϕ05 wing models are shown. The moment coefficient was drawn from the trailing edge to amplify the effects of the leading-edge modifications.

The drag coefficient in the upper left plot of Fig. 3 shows only a slight difference among the wing models at the lower angles of attack. The rate of change of the drag coefficient is similar for all the wing models until the angle-of-attack reaches $\alpha = 17^\circ$. As the angle-of-attack exceeds $\alpha = 17^\circ$, the rate of change of the drag coefficient decreases for all the wing models. However, the corresponding rate of change for the base wing model decreases more significantly than that of the modified wing models. Among the modified wing models, the S-λ2ϕ03 model indicates the greatest decrease, while the ST-λ2ϕ05 model shows the least decrease in the rate of change.

Considering the lift coefficient distribution, as shown in the lower left plot of Fig. 3, increases in the stall angle and the maximum lift coefficient ($C_{L\,\max}$) value for the modified wings is evident. The base wing model shows stall characteristics around $\alpha = 17^\circ$ with a $C_{L\,\max} = 0.73$. Among the modified wings, the S-λ2ϕ05 and ST-λ2ϕ05 models demonstrated the best stall-delaying abilities, both stalling around $\alpha = 21^\circ$. The S-λ2ϕ05 model had a $C_{L\,\max} = 0.75$, and the ST-λ2ϕ05 model had a $C_{L\,\max} = 0.77$. The S-λ2ϕ03 model stalled around $\alpha = 19^\circ$ with a $C_{L\,\max} = 0.76$. The decrease in the lift coefficient post-stall of the modified wing models was not as drastic as that of the base wing model, showing smoother stall characteristics. A smoother stall behaviour and higher stall angles increase the range of angle-of-attack

https://doi.org/10.1017/aer.2025.10071 Published online by Cambridge University Press

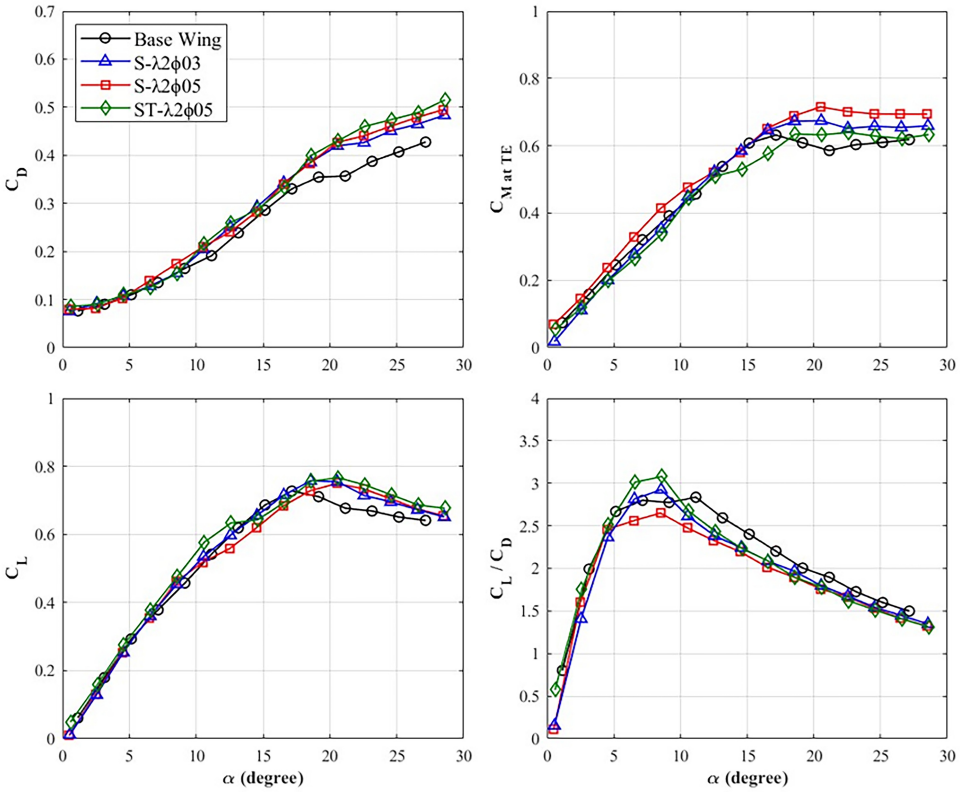

Figure 3. *Drag coefficient (C_D), lift coefficient (C_L), moment coefficient (C_M), and the lift-to-drag ratio (C_L/C_D) at various angles of attack for different wing models.*

at which manoeuverability is enhanced [30]. Moreover, there is an increase in the lift coefficient of the modified wing models compared to the base wing post-stall. The rate of change of the lift coefficient is similar for all the wing models until $\alpha = 9°$. The ST-λ2ϕ05 wing model shows a higher rate of change of lift coefficient between the angles of attack of 9° and 13°. In contrast, the rate of change decreases for the S-λ2ϕ05 wing model between the angles of attack of 9° and 13°. As the angle-of-attack exceeds $\alpha = 13°$, the rate of change is similar for all the wing models until their corresponding stall angle.

For further discussion of the drag and lift coefficients for modified wings, it is important to note that the S-λ3ϕ05 and S-λ2ϕ05 wing models share the same amplitude ratio of $\phi/C = 0.05$ and have wavelength ratios of $\lambda/C = 0.3$ and $\lambda/C = 0.2$, respectively. As the angle-of-attack exceeds $\alpha = 21°$ an increase in the drag coefficient is present in the wing model with the lower wavelength ratio. The wing model with a higher wavelength ratio showed higher lift coefficient values when the angle-of-attack is between $\alpha = 11°$ and $\alpha = 21°$. No significant effect of the wavelength ratio was observed in other angles of attack. In addition, S-λ2ϕ03 and S-λ2ϕ05 wing models share the same wavelength ratio of $\lambda/C = 0.2$ and have amplitude ratios of $\phi/C = 0.03$ and $\phi/C = 0.05$, respectively. As the angle-of-attack surpasses $\alpha = 21°$ an increase in the drag coefficient is present in the wing model with the higher amplitude ratio. The wing model with a higher amplitude ratio showed lower lift coefficient values when the angle-of-attack is between $\alpha = 11°$ and $\alpha = 21°$. No significant effect of the amplitude ratio was observed in other angles of attack.

Considering the moment coefficient at the trailing edge, as shown in the upper right plot of Fig. 3, a similar positive slope for wing models at the lower angles of attack is witnessed. The S-λ2ϕ05 wing model shows higher slope values between the angles of attack of 5° and 11° compared to the other wing models. As the angle-of-attack exceeds $\alpha = 13°$, the slope of the ST-λ2ϕ05 model decreases while the slopes of other wing models remain unchanged until $\alpha = 17°$. The slope of the base wing model

https://doi.org/10.1017/aer.2025.10071 Published online by Cambridge University Press

becomes negative when the angle-of-attack is past $\alpha = 17°$. In contrast, the slopes of the modified wing models remained positive until approximately $\alpha = 21°$. Even when the slope of the modified wing models becomes negative, the slope does not decrease drastically compared to the base wing. Modified wing models showed near neutral stability past $\alpha = 21°$, while the base wing model demonstrated alternating stability around $\alpha = 21°$. Considering post-stall characteristics of the drag and lift coefficients, higher linearity is observed for both coefficients for modified wings compared to the base wing, in return contributing smoother stability characteristics, whereas the base wing exhibits alternating stability characteristics after stall. The angle range aforementioned in lift coefficient results, where manoeuverability is enhanced, coincides with the moment coefficient results.

The lift-to-drag ratio (C_L/C_D) is a key indicator of the aerodynamic performance of a wing model. This ratio is displayed in the lower right plot of Fig. 3. The lift-to-drag ratio remains similar for all the wing models until the angles of attack of $\alpha = 5°$. Between $\alpha = 5°$ and $\alpha = 9°$, the ST-λ2ϕ05 and S-λ2ϕ03 models demonstrate better aerodynamic performance, making them more suitable for cruise conditions. Moreover, all modified wing models reach their maximum lift-to-drag ratio at lower angles of attack compared to the base wing, further enhancing their desirability for cruise conditions. However, the base wing model outperforms the modified wing models for angles of attack greater than $\alpha = 9°$. The peak value of the lift-to-drag ratio was observed at lower angles of attack for modified wing models, showing more desired conditions for cruise conditions.

These observations regarding the stall-delaying capabilities of the bio-inspired wing models were in line with those in the works of Chen et al. [3] and Ramakrishna et al. [26]. Moreover, the sinusoidal leading-edge on aerofoils by Miklosovic et al. [20], Post et al. [25], Câmara and Sousa [2], and Moscato et al. [21] showed similar stall-delaying capabilities. The increase in the drag and lift coefficients witnessed in this study for the bio-inspired wing modifications at post-stall of the base wing aligns with the findings of the delta wing studies by Chen et al. [3] and aerofoil studies by Post et al. [25], Moscato et al. [21], Ntantis et al. [24], and Liu et al. [18]. Post et al. [25], Johari et al. [14], Hansen et al. [13], Miklosovic et al. [19, 20].

However, some aerofoil studies conducted by Johari et al. [14] and Guerreiro and Sousa [8] indicated a lower lift prior to the base wing's stall angle, which might be due to the differences in wavelengths and Reynolds numbers used in these studies.

3.2 Results of surface pressure measurements

The results of the surface pressure measurements are presented in Fig. 4, showing distributions of negative pressure coefficient ($-C_p$) for the base wing, S-λ2ϕ03, S-λ2ϕ05 and ST-λ2ϕ05 wing models at various angles of attack with respect to the spanwise distance (y/s), where s is the half-span at the chordwise location $x/C = 0.5$.

At low angles of attack, there is a typical S-shaped $-C_p$ distribution for the base wing, S-λ2ϕ03, and S-λ2ϕ05 models, indicating the presence of a leading-edge vortex and its footprint on the wing surface. However, the ST-λ2ϕ05 wing model exhibits a different behaviour, such that the pressure coefficient is generally constant except for the regions very close to the leading edge. The lift coefficient results of this wing were higher than other wing models at $\alpha = 11°$; however, it shows smaller suction regions compared to other wing models at this angle-of-attack. This might indicate a strong leading-edge vortex present inward of the delta wing, providing higher lift compared to other wing models.

As the angle-of-attack increases from $\alpha = 7°$ to $\alpha = 9°$, the suction pressure peak shifts slightly inboard for the S-λ2ϕ03 wing model. For the S-λ2ϕ05 wing model, the suction peak moves more noticeably as the angle-of-attack increases from $\alpha = 7°$ to $\alpha = 11°$. In contrast, the suction peak of the ST-λ2ϕ05 wing model remains largely stationary until just before $\alpha = 15°$. For the base wing model, the suction peak does not experience significant movements until approximately $\alpha = 19°$.

The maximum suction pressure of the modified wing models increases up to approximately $\alpha = 17°$. Further increases in the angle-of-attack result in a decrease in suction pressure. Around $\alpha = 19°$, the pressure distribution for the base wing model levels off, indicating the onset of stall, due to the three-dimensional surface separation. In contrast, the modified wing models do not completely flatten out

https://doi.org/10.1017/aer.2025.10071 Published online by Cambridge University Press

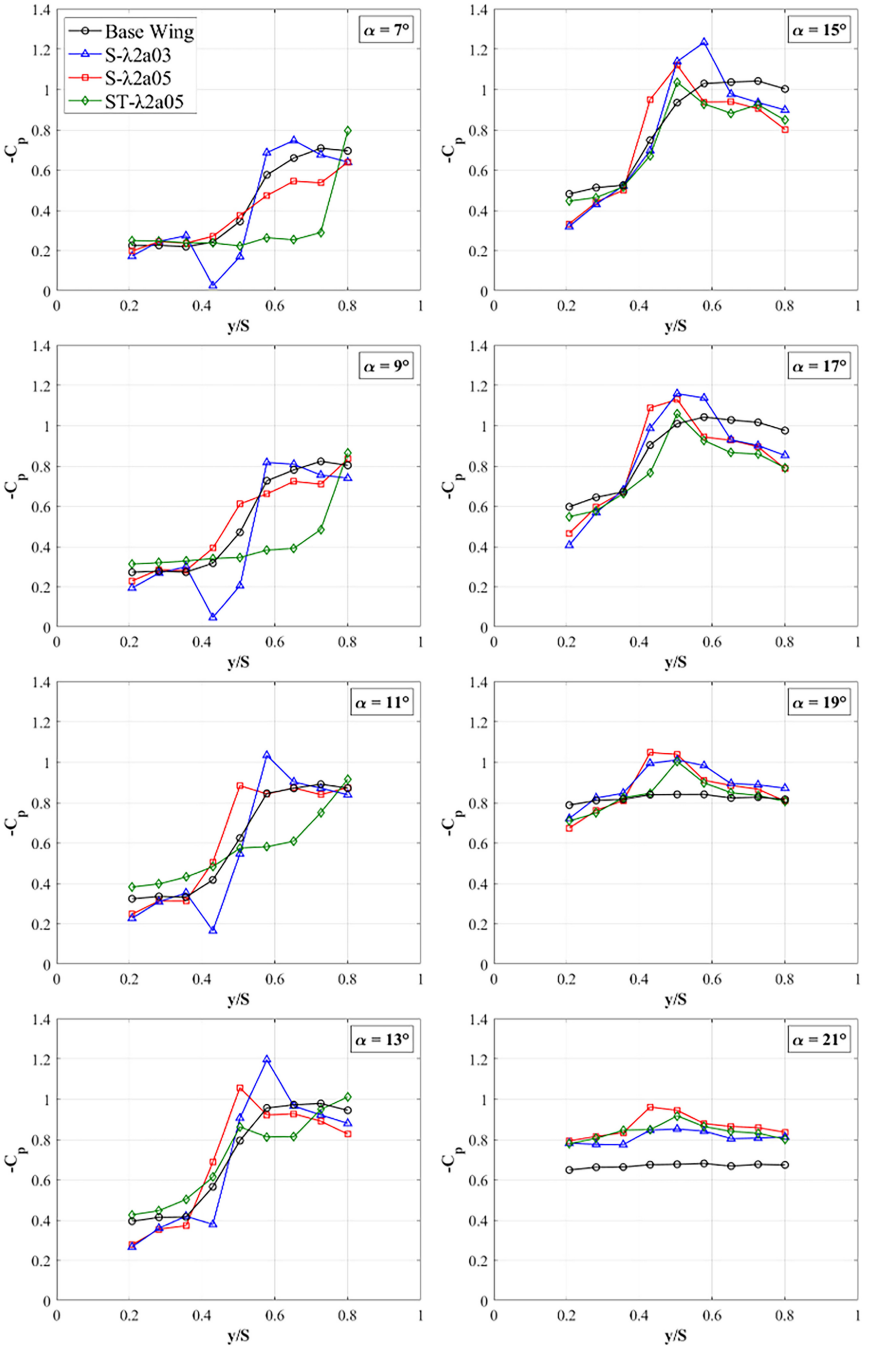

Figure 4. *Distribution of pressure coefficient at various angles of attack for different wing models on half span at* $x/C = 0.5$.

the pressure distribution even at $\alpha = 21^{\circ}$, indicating that the flow has not fully separated from the wing surface. The magnitudes of the $-C_p$ values are significantly higher for modified wing models, indicating stronger suction pressure and, consequently, higher lift.

Figure 5 presents the distribution of pressure coefficients for the base, S-λ2ϕ03, S-λ2ϕ05, and ST-λ2ϕ05 wing models at the three angles of attack closest to the stall angles identified from the force

https://doi.org/10.1017/aer.2025.10071 Published online by Cambridge University Press

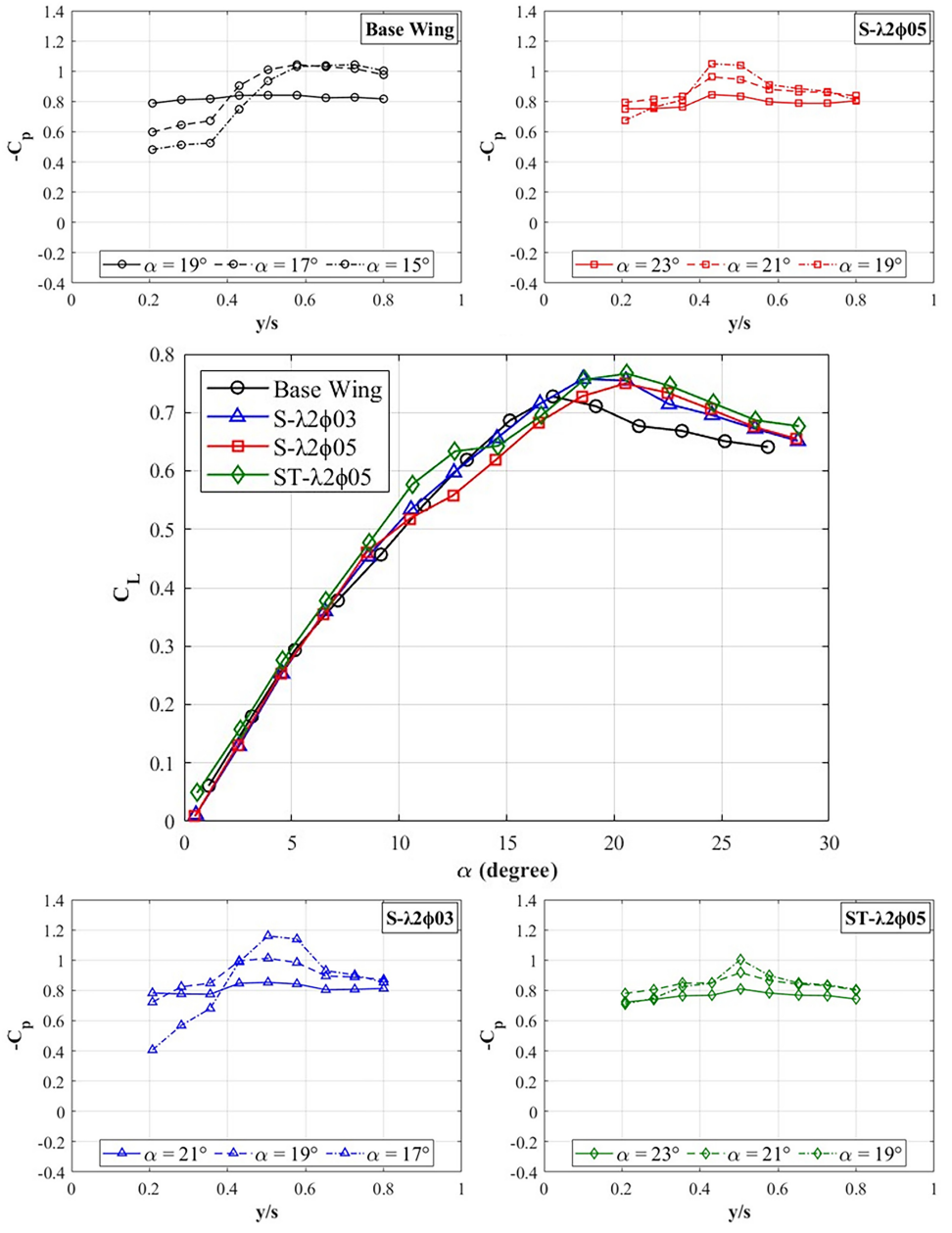

Figure 5. *Distribution of pressure coefficient at various angles of attack, along with the lift coefficient comparison for different wing configurations.*

measurements of each respective wing model, along with the comparison of their lift coefficients. The indications of delayed stall onset from the force measurements are consistent with those observed from the surface pressure measurements.

4.0 Conclusions

The effect of bio-inspired leading-edge modifications on the aerodynamic performance of a non-slender delta wing with a sweep angle of $\Lambda = 45°$ was presented in the current study. Four sinusoidal and two

https://doi.org/10.1017/aer.2025.10071 Published online by Cambridge University Press

saw-tooth leading-edge wing models with different wavelength and amplitude ratios were compared with a base wing model. Force and surface pressure measurements were performed at a Reynolds number of $Re = 1 \times 10^5$ over a wide angle-of-attack range in a low-speed wind tunnel. The main findings of this study regarding the force and surface pressure measurements are:

1. Force measurement results revealed that utilising bio-inspired leading-edge modifications delayed stall and increased the maximum lift coefficient ($C_{L\,\max}$) value. Moreover, the bio-inspired wing models showed an increased lift coefficient compared to the base wing model over the angle-of-attack of $\alpha = 17°$, providing smoother stall characteristics. The S-$\lambda 2\phi 05$ and ST-$\lambda 2\phi 05$ models delay stall up to 4 degrees, both stalling around $\alpha = 21°$. Pressure measurement results showed delayed stall onset for the modified wings, supporting the claims of the force measurements. The ST-$\lambda 2\phi 05$ wing model demonstrated smaller suction regions, hence lower lift generation capability at $\alpha = 11°$, while having the highest lift coefficient among all the wing models at this angle-of-attack. This indicates a high promotion of leading-edge vortices at lower angles of attack.
2. There is no significant difference in the drag, lift and moment coefficient among the wing models below $\alpha = 10°$. However, the lift-to-drag coefficient significantly differs among the wing models as the angle-of-attack exceeds $\alpha = 5°$. As the angle-of-attack increases over $\alpha = 17°$, an increase in the drag, lift and moment coefficient for the modified wing models compared to the base wing model is apparent. When the lift-to-drag ratio is considered, the ST-$\lambda 2\phi 05$ and S-$\lambda 2\phi 03$ models show better aerodynamic performance between $\alpha = 6°$ and $\alpha = 9°$. The base wing model shows better aerodynamic performance than the modified wings as the angle-of-attack increases further, yet the difference is minor.
3. The moment coefficient results demonstrated similar slopes for all the wing models at the lower angles of attack. However, as the angle-of-attack increases further, S-$\lambda 2\phi 05$ and ST-$\lambda 2\phi 05$ wing models show distinct behaviours. The S-$\lambda 2\phi 05$ wing model indicates lower stability between the angles of attack from 5° to 11°, and the ST-$\lambda 2\phi 05$ wing model shows higher stability between the angles of attack of 11° to 19°, compared to other wing models. The bio-inspired wing models generally showed a lower longitudinal static stability as the angle-of-attack surpassed $\alpha = 17°$. Bio-inspired leading-edge modifications can improve the manoeuverability of an aircraft and can be utilised in various applications, since these modifications provide higher lift, smoother stall characteristics and lower negative rate of change in moment coefficient. A reduction in longitudinal static stability at high angles of attack can enhance manoeuverability, which is advantageous in air combat scenarios. However, for non-slender delta wings operating at low speeds, such reductions must be carefully balanced to preserve adequate control authority and ensure acceptable handling qualities.

Competing interests. No conflict of interest.

References

[1] Anders, J. Biomimetic flow control, *AIAA J.*, 2000 https://doi.org/10.2514/6.2000-2543
[2] Câmara, J.F.D. and Sousa, J.M.M. Numerical study on the use of a sinusoidal leading edge for passive stall control at low Reynolds number, 51st AIAA Aerospace Sciences Meeting, 2013. https://doi.org/10.2514/6.2013-62
[3] Chen, H., Pan, C. and Wang, J. Effects of sinusoidal leading edge on delta wing performance and mechanism, *Sci. China Technol. Sci.*, 2013, **56**, (3), pp 772–779. https://doi.org/10.1007/s11431-013-5143-3
[4] Chen, H. and Wang, J.J. Vortex structures for flow over a delta wing with sinusoidal leading edge, *Exp. Fluids*, 2014, **55,** (6). https://doi.org/10.1007/s00348-014-1761-1
[5] Domel, A.G., Saadat, M., Weaver, J.C., Haj-Hariri, H., Bertoldi, K. and Lauder, G.V. Shark skin-inspired designs that improve aerodynamic performance, *J. R. Soc. Interface*, 2018, **15,** (139). https://doi.org/10.1098/rsif.2017.0828
[6] Fish, F.E., Weber, P.W., Murray, M.M. and Howle, L.E. The tubercles on humpback whales' flippers: Application of bio-inspired technology, *Integr. Comp. Biol.*, 2011, **51,** (1), pp 203–213. https://doi.org/10.1093/icb/icr016
[7] Goruney, T. and Rockwell, D. Flow past a delta wing with a sinusoidal leading edge: Near-surface topology and flow structure, *Exp. Fluids*, 2009, **47,** (2), pp 321–331. https://doi.org/10.1007/s00348-009-0666-x

https://doi.org/10.1017/aer.2025.10071 Published online by Cambridge University Press

[8] Guerreiro, J.L.E. and Sousa, J.M.M. Low-Reynolds-number effects in passive stall control using sinusoidal leading edges, *AIAA J.*, 2012, **50,** (2), pp 461–469. https://doi.org/10.2514/1.J051235
[9] Gupta, S., Kumar, S. and Kumar, R. Control of leading-edge vortices over delta wing using flow control methods: A review, *Mater. Today Proc.*, 2022, **50**, pp 2189–2193.
[10] Gursul, I. Recent developments in delta wing, *Aeronaut. J.*, 2004, **108**, pp 437–452.
[11] Gursul, I., Cleaver, D.J. and Wang, Z. Control of low Reynolds number flows by means of fluid-structure interactions, *Progr. Aerospace Sci.*, 2014, **64**, 17–55. https://doi.org/10.1016/j.paerosci.2013.07.004
[12] Gursul, I., Gordnier, R. and Visbal, M. Unsteady aerodynamics of nonslender delta wings, *Progr. Aerospace Sci.*, 2005, **41,** (7), 515–557. https://doi.org/10.1016/j.paerosci.2005.09.002
[13] Hansen, K., Kelso, R.M. and Dally, B. An investigation of three-dimensional effects on the performance of tubercles at low Reynolds numbers, *17th Australasian Fluid Mechanics Conference*, 2010. https://www.researchgate.net/publication/267700453
[14] Johari, H., Henoch, C., Custodio, D. and Levshin, A. Effects of leading-edge protuberances on airfoil performance, *AIAA J.*, 2007, **45**, (11), pp 2634–2642. https://doi.org/10.2514/1.28497
[15] Kim, M.J., Yoon, H.S., Jung, J.H., Chun, H.H. and Park, D.W. Hydrodynamic characteristics for flow around wavy wings with different wave lengths, *Int. J. Naval Arch. Ocean Eng.*, 2012, **4,** (4), pp 447–459. https://doi.org/10.2478/ijnaoe-2013-0110
[16] Lee, S.I., Kim, J., Park, H., Jabłoński, P.G. and Choi, H. The function of the alula in avian flight, *Sci. Rep.*, 2015, **5**. https://doi.org/10.1038/srep09914
[17] Lilienthal, O. *Birdflight as the Basis of Aviation*. Longmans, Green, and Co., 1911.
[18] Liu, K., Song, B., Xue, D., Yang, W., Chen, A. and Wang, Z. Numerical study of the aerodynamic effects of bio-inspired leading-edge serrations on a heaving wing at a low Reynolds number, *Aerospace Sci. Technol.*, 2022, **124**. https://doi.org/10.1016/j.ast.2022.107529
[19] Miklosovic, D.S., Murray, M.M. and Howle, L.E. Experimental evaluation of sinusoidal leading edges, *J. Aircraft*, 2007, **44**(4), pp 1404–1408. https://doi.org/10.2514/1.30303
[20] Miklosovic, D.S., Murray, M.M., Howle, L.E. and Fish, F.E. Leading-edge tubercles delay stall on humpback whale (Megaptera novaeangliae) flippers, *Physics of Fluids*, 2004, **16,** (5). https://doi.org/10.1063/1.1688341
[21] Moscato, G., Mohamed, J. and Romano, G.P. Improving performances of biomimetic wings with leading-edge tubercles, *Experiments in Fluids*, 2022, **63,** (9). https://doi.org/10.1007/s00348-022-03493-8
[22] Muthuramalingam, M., Villemin, L.S. and Bruecker, C. Streak formation in flow over biomimetic fish scale arrays, *J. Exp. Biol.*, 2019, **222,** (16). https://doi.org/10.1242/jeb.205963
[23] Naeini, H.K., Nili-Ahmadabadi, M., Park, Y.S. and Kim, K.C. Effect of nature-inspired needle-shaped vortex generators on the aerodynamic features of a double-delta wing, *Int. J. Mech. Sci.*, 2021, pp 202–203. https://doi.org/10.1016/j.ijmecsci.2021.106502
[24] Ntantis, E.L., Francis, E., Pugazendi, V., George, J., Tarek, A., Emthias, M. and Rasheed, S. Study of sinusoidal perturbations on the leading edge of an aircraft wing, *J. Aeronaut. Astronaut. Aviat.*, 2021, **53,** (3), pp 375–386. https://doi.org/10.6125/JoAAA.202109_53(3).04
[25] Post, M.L., Decker, R., Sapell, A.R. and Hart, J.S. Effect of bio-inspired sinusoidal leading-edges on wings, *Aerospace Sci. Technol.*, 2018, **81**, pp 128–140. https://doi.org/10.1016/J.AST.2018.07.043
[26] Ramakrishna, M., Senthil Kumar, C. and Venkatesh, B. Influence of leading edge shapes on vortex behaviour of delta wing, *J. Phys. Conf. Ser.*, 2019, **1276,** (1).
[27] Rao, C. and Liu, H. Effects of Reynolds number and distribution on passive flow control in owl-inspired leading-edge serrations, *Integr. Comp. Biol.*, 2020, **60,** (5), pp 1135–1146. https://doi.org/10.1093/ICB/ICAA119
[28] Rose, J.B.R., Natarajan, S.G. and Gopinathan, V.T. Biomimetic flow control techniques for aerospace applications: a comprehensive review, in *Reviews in Environmental Science and Biotechnology*, Vol. **20**(3). Springer, 2021, pp. 645–677. https://doi.org/10.1007/s11157-021-09583-z
[29] Shahsavari, A., Nili-Ahmadabadi, M., Aslani, A. and Kim, K.C. Introduction of a biomimetic device designed to improve the flow over a slender delta wing: Visualization study, *J. Visualization*, 2024 https://doi.org/10.1007/s12650-024-00961-7
[30] van Nierop, E.A., Alben, S. and Brenner, M.P. How bumps on whale flippers delay stall: An aerodynamic model, *Phys. Rev. Lett.*, 2008, **100,** (5). https://doi.org/10.1103/PhysRevLett.100.054502
[31] Yoon, H.S., Hung, P.A., Jung, J.H. and Kim, M.C. Effect of the wavy leading edge on hydrodynamic characteristics for flow around low aspect ratio wing, *Comput. Fluids*, 2011, **49,** (1), pp 276–289. https://doi.org/10.1016/j.compfluid.2011.06.010
[32] Zhao, M., Wei, T., Zhao, Y. and Liu, Z. Influences of leading-edge tubercle amplitude on airfoil flow field, *J. Therm. Sci.*, 2023, **32,** (4), pp 1335–1344. https://doi.org/10.1007/s11630-023-1465-z
[33] Zverkov, I., Zanin, B. and Kozlov, V. Disturbances growth in boundary layers on classical and wavy surface wings, *AIAA J.*, 2008, **46,** (12), pp 3149–3158. https://doi.org/10.2514/1.37562

Cite this article: Dikbaş D., Güneş E., Koçak G. and Yavuz M. M. Effect of bio-inspired leading-edge modifications on aerodynamic performance of a non-slender delta wing. *The Aeronautical Journal*, https://doi.org/10.1017/aer.2025.10071